Journal of Power Sources 232 (2013) 370–375

Contents lists available at SciVerse ScienceDirect

Journal of Power Sources

journal homepage: www.elsevier.com/locate/jpowsour

Effect of Al-doped β-Ni(OH)$_2$ nanosheets on electrochemical behaviors for high performance supercapacitor application

Jichun Huang, Ting Lei, Xiaopei Wei, Xinwei Liu, Tong Liu, Dianxue Cao, Jinling Yin, Guiling Wang*

Key Laboratory of Superlight Material and Surface Technology of Ministry of Education, College of Material Science and Chemical Engineering, Harbin Engineering University, Harbin 150001, PR China

HIGHLIGHTS

- Al-doped β-Ni(OH)$_2$ nanosheets were prepared by a simple hydrothermal process.
- The effect of Al content on the electrochemical behaviors was investigated clearly.
- The as-prepared $Al_{0.034}Co_{0.966}$LDH electrode exhibited highest specific capacitance of 2122.6 F g^{-1} at 1 A g^{-1}.

ARTICLE INFO

Article history:
Received 26 November 2012
Received in revised form
31 December 2012
Accepted 14 January 2013
Available online 22 January 2013

Keywords:
Nickel hydroxide
Aluminum
Nickel foam
Supercapacitor

ABSTRACT

Al-doped β-Ni(OH)$_2$ nanosheets are prepared by a simple hydrothermal process onto nickel foam by using a mixed aqueous solution of nickel nitrate, aluminum nitrate and ammonia. Their structure and surface morphology are studied by using X-ray diffraction analysis, energy-dispersive X-ray spectroscopy and scanning electron microscopy. The SEM images show changes in the microstructure of β-Ni(OH)$_2$ by the addition of Al. The XRD results show that the α-phase Ni(OH)$_2$ appeared by the addition of Al. The effects of Al content on the electrochemical behaviors of β-Ni(OH)$_2$ are investigated by cyclic voltammetrys, galvanostatic charge/discharge and electrochemical impedance spectroscopy. The results show a drastic improvement in the capacitive characteristics of β-Ni(OH)$_2$ with a specific capacitance increase from 941.7 to 2122.6 F g^{-1} by the addition of just 3.4 mol% Al. This work suggests that the as-prepared $Al_{0.034}Ni_{0.966}$LDH electrode has a promising future as higher charging/discharging rate materials for pseudo-supercapacitors.

1. Introduction

Electrochemical capacitors (ECs) or supercapacitors are attracting significant attention as energy efficient, eco-friendly, high-power, high-energy devices. Their long cycle life, excellent safety and eco-friendly nature are highly advantageous in offering alternatives to fossil-fuel, and thus they can contribute significantly in controlling global warming [1–3]. ECs can be categorized into two main types on the basis of their charge-storage mechanisms: (1) electrical double layer capacitors (EDLCs), where the electrical charge is stored at the interface between the electrode and the electrolyte; (2) redox electrochemical capacitors, where capacitance arises from faradic reactions taking place at the electrode/electrolyte interface [2,3]. For EDLCs, the most common supercapacitors at present, use carbon-based materials (activated carbons, carbon nanotubes, and reduced graphene oxide) [4,5] with high surface area as the electrode materials, while pseudocapacitors use transition-metal oxides/hydroxides (RuO_2 [6], MnO_2 [7,8], CuO [9,10], Fe_2O_3 [11,12],Co_3O_4 [13–15], Co(OH)$_2$ [16,17], NiO [18], Ni(OH)$_2$ [19,20]) or conducting polymers (polyaniline, polypyrrole, and polythiophene) [21,22] as active materials. However, each material has its unique advantages and disadvantages for ECs application. For example, carbon material has high power density and long life cycle, but the small double-layer capacitance limits its application. Transition-metal oxides/hydroxides and conducting polymers have been widely investigated due to their relatively higher capacitance and fast redox kinetics, while the relatively low mechanical stability and cycle life are major limitations for ECs.

In recently, many researches were conducted to investigate the layered double hydroxides (LDH) materials. LDH materials are lamellar compounds with the chemical formula $[M_a(II)_{1-x}M_b(III)_x(OH)_2]^{x+}[A^{n-}]_{x/n} \times mH_2O$, shortly named $M_a/M_b - A$, where M_a(II) and M_b(III) are metal cations, A^{n-} is an anion [23,24]. Due to their anion exchange property and capacity to intercalate anions, LDH materials have been widely

* Corresponding author. Tel./fax: +86 451 82589036.
E-mail address: wangguiling@hrbeu.edu.cn (G. Wang).

0378-7753/$ – see front matter © 2013 Elsevier B.V. All rights reserved.
http://dx.doi.org/10.1016/j.jpowsour.2013.01.081

employed in catalysts, anion exchangers, precursors to oxides, magnetics, and electrodes for alkaline secondary batteries [23]. Recently, LDH materials containing transition metals have been reported to be promising electrode materials for ECs because of their relatively low cost, high redox activity, and environmentally friendly nature [25–28]. Recently, Gao et al. used a facile hydrothermal technique to synthesize graphene nanosheet/$Ni^{2+}Al^{3+}$/LDH composite with excellent surface area and microstructure. The as-prepared graphene nanosheet/$Ni^{2+}Al^{3+}$/LDH composite electrode displayed a high specific capacitance of 781.5 F g^{-1} at 5 mV s^{-1} [25]. Lu et al. investigated the supercapacitor performance of Co/Al-LDH nanosheet arrays prepared by a simple hydrothermal method. The Co/Al-LDH nanosheet arrays electrode exhibits enhanced specific capacitance (1075 F g^{-1} at 5 mA cm^{-2}) and higher rate capability and cycling stability (92% maintained after 2000 cycles) [28]. To the best of our knowledge, Gupta's group [26,27] prepared $Co_xNi_yAl_z$ layered triple hydroxides electrodes with nanostructures which displayed the maximum specific capacitances of 1263 F g^{-1} at present. The enhanced supercapacitor performances are due to their unique LDH structure providing fast ion and electron transfer, large reaction surface area and good electrochemical activity [23,29].

In this study, Al-doped β-$Ni(OH)_2$ LDH electrode has been successfully synthesized on nickel foam by a simple hydrothermal method. The effect of the contents of Al on the electrochemical performance has also been investigated. The as-obtained $Al_{0.034}Co_{0.966}$LDH electrode exhibited highest specific capacitance of 2122.6 F g^{-1} at 1 A g^{-1} and excellent long cycle life.

2. Experimental

2.1. Preparation and characterization of Al_xNi_{1-x}LDH electrode

All the chemicals are of analytical grade and were used without further purification. The electrode of β-$Ni(OH)_2$ nanosheets on nickel foam were synthesized according to the previous procedures described in our literature [30]. The Al-doped β-$Ni(OH)_2$ electrode was prepared by adding the aluminum nitrate in the reaction solution. Briefly, 10 mmol $Ni(NO_3)_2{\cdot}6H_2O$ and $Al(NO_3)_3{\cdot}9H_2O$ were dissolved in 35 cm^3 H_2O + 15 cm^3 ammonia (25–28 wt%). The solution was magnetically stirred for 15 min at room temperature and heated at 90 °C for 2 h (growth ready solution). The pretreated nickel foam was immersed in the growth solution for 12 h at 90 °C for the growth of nanosheets. After growth, the electrode was washed and heated at 60 °C to obtain the final electrode. The morphology was examined by scanning electron microscope (SEM, JEOL JSM-6480) equipped with an energy-dispersive X-ray (EDX) analyzer. The structure of the products was analyzed using X-ray diffractometer (XRD, Rigaku TTR III) with Cu K_α radiation ($\lambda = 0.1506$ nm). The 2θ ranges from 5° to 90° with a scan rate of 10° min^{-1} and a step width of 0.02°.

2.2. Electrochemical measurements

The cyclic voltammetrys (CVs), galvanostatic charge–discharge and electrochemical impedance spectroscopy (EIS) tests were performed in a conventional three-electrode electrochemical cell using a computerized potentiostat (VMP3/Z Bio-Logic) controlled by the EC-lab software. The as-prepared electrode (1 cm^2 nominal planar area) acted as the working electrode, a platinum foil (1 × 2 cm^2) served as the counter electrode, and a saturated calomel electrode (SCE) was used as the reference electrode. The cycle life tests were conducted on a LAND battery program-control test system. All electrochemical measurements were performed in 6 mol dm^{-3} KOH. The solutions were made with analytical grade chemical reagents and Milli-Q water (18 MΩ cm, Millipore). EIS measurements were performed by applying an AC voltage with 5 mV amplitude in a frequency range from 0.01 Hz to 100 kHz at the open circuit potential.

3. Results and discussion

3.1. Characterization of the Al_xNi_{1-x}LDH electrode

The mol content of Al in the initial solution as well as in the prepared Al-doped β-$Ni(OH)_2$ LDH electrode, obtained by means of EDX analysis, are given in Table 1. It can be seen that the content of substituted Al is proportional to that in the initial solution. In the following text, the Al-doped β-$Ni(OH)_2$ LDH are abbreviated as Al_xNi_{1-x}LDH, with $x = 0.013$, 0.019, and 0.034. It was found that the mol content of Al increases with the increase in the initial solution, revealing the substitution of Ni of the materials. It should be pointed that when the mol content of Al in the initial solution was conducted beyond 7 mol%, the homogeneous Al_xNi_{1-x}LDH electrode was not obtained by this method. This is why in the article only 3 mol%, 5 mol% and 7 mol% are presented.

Fig. 1 shows the XRD patterns of β-$Ni(OH)_2$ and Al_xNi_{1-x}LDH ($x = 0.013$, 0.019, and 0.034). Before the addition of Al, the XRD pattern matches well with the standard crystallographic spectrum of hexagonal β-$Ni(OH)_2$ (JCPDS card No. 14-0117). The lattice constants were calculated to be $a = b = 0.3121$ nm and $c = 0.4611$ nm for the sample; they are consistent with the standard values of β-$Ni(OH)_2$ ($a = b = 0.3126$ nm, and $c = 0.4605$ nm). The effect of Al^{3+} can be noticed in the X-ray diffraction patterns. It was found that the typical diffraction peaks of α-phase $Ni(OH)_2$ (JCPDS card No. 38-0715) appeared with the addition of Al. As the mol content of Al in β-$Ni(OH)_2$ was increased, the diffraction intensity of α-phase $Ni(OH)_2$ increased slightly, while the diffraction intensity of β-phase $Ni(OH)_2$ decreased slightly. For Al_xNi_{1-x}LDH ($x = 0.013$, 0.019, and 0.034), the lattice constants were calculated to be $a = 0.3120$ nm, 0.3118 nm, 0.3095; and $c = 0.4622$ nm, 0.4634 nm, 0.4678 nm, respectively. It can be seen that the parameter of a decreases gradually with increasing Al in nickel hydroxides. This is due to the difference of metal ionic radius between aluminum and nickel. The radius of Al^{3+} ions is 0.54 Å, smaller than the radius of Ni^{2+} (0.69 Å) in the lattice of nickel hydroxides [32] The value of interlayer distance increases slightly for the Al_xNi_{1-x}LDH because of intercalated species (water and anions) within the interlayer of nickel hydroxide [33,34] It was noted that the position of diffraction peak (003) of Al_xNi_{1-x}LDH shifted left slightly with the increase of Al contents. However, the substitution of Al did not affect the crystal structure of β-phase $Ni(OH)_2$ significantly.

Fig. 2 shows the SEM images of β-$Ni(OH)_2$ and Al_xNi_{1-x}LDH ($x = 0.013$, 0.019, and 0.034) attached on the nickel foam. The SEM image (Fig. 2a) shows that β-$Ni(OH)_2$ presents on the nickel foam skeleton partially as spherical clusters, which are actually composed of nanosheets. When the mol content of Al substitution in β-$Ni(OH)_2$ was 1.3 mol% ($Al_{0.013}Ni_{0.987}$LDH), a decrease in the thickness of the nanosheets was observed (Fig. 2b). For the Al substitution of 1.9 mol% ($Al_{0.019}Ni_{0.981}$LDH), the active material attached on the nickel foam was converted to uniform film (Fig. 2c). No obvious changes were observed upon increasing the Al substitution up to 3.4 mol% ($Al_{0.034}Ni_{0.966}$LDH), as shown in Fig. 2d.

Table 1
EDX analysis of Al content in β-$Ni(OH)_2$ as compared to Al content in the initial molar solutions of $Ni(NO_3)_2{\cdot}6H_2O$ and $Al(NO_3)_3{\cdot}9H_2O$.

Sample No.	Al content in solution [Al/Co + Al] (mol%)	Al content in sample [Al/Co + Al] (mol%)
1	3	1.3
2	5	1.9
3	7	3.4

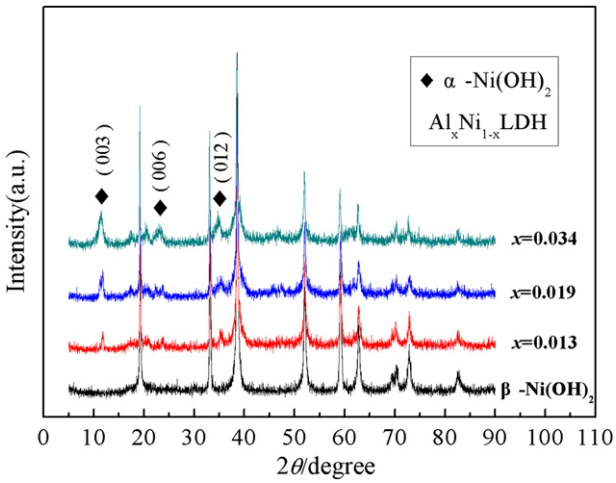

Fig. 1. XRD patterns of $Al_xNi_{1-x}LDH$ with x values of (a) 0, (b) 0.013, (c) 0.019, (d) 0.034.

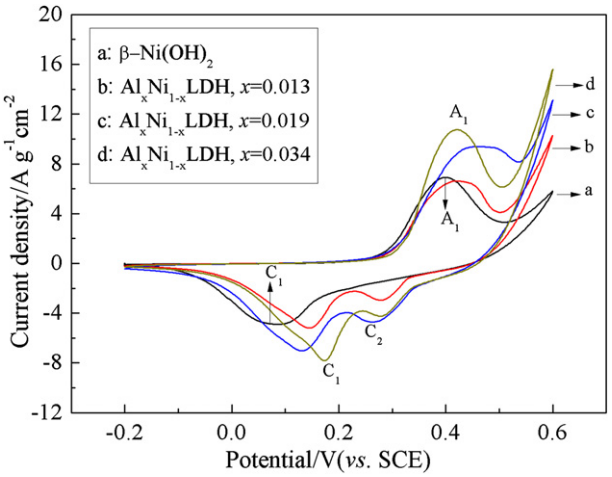

Fig. 3. The CVs of the $Al_xNi_{1-x}LDH$ electrode at a scan rate of 2 mV s^{-1} in the potential range of −0.2–0.6 V.

3.2. Supercapacitance performance of the $Al_xNi_{1-x}LDH$ electrode

Fig. 3 shows the CVs of the β-$Ni(OH)_2$, $Al_{0.013}Ni_{0.987}LDH$, $Al_{0.019}Ni_{0.981}LDH$, and $Al_{0.034}Ni_{0.966}LDH$ in 6.0 mol dm^{-3} KOH solution at a scan rate of 2 mV s^{-1}. For pure β-$Ni(OH)_2$, obvious the anodic peaks (A_1) and cathodic peaks (C_1) were observed in the potential range of −0.2–0.6 V. The peaks can be attributed to the transition of the redox couple β-$Ni(OH)_2$/β-NiOOH, indicating that the electrochemical capacitance of the β-$Ni(OH)_2$ electrode mainly results from the pseudocapacitance [29]. The oxidation and reduction potential peaks (A_1 and C_1) of pure β-$Ni(OH)_2$ electrode are located at 404 mV and 71 mV. While the oxidation and reduction potential peaks (A_1 and C_1) of $Al_xNi_{1-x}LDH$ electrode shift more positive position. After the addition of Al, the additional cathodic peak (C_2) occurred at more positive potential position compared to the cathodic peak (C_1). In the sample of $Al_{0.034}Ni_{0.966}LDH$, the first small cathodic peak appears at 172 mV, corresponding to the reduction reaction process from γ-NiOOH to α-$Ni(OH)_2$. While the second cathodic peak appear at 277 mV, relating to the process from β-NiOOH to β-$Ni(OH)_2$ [29]. With the increase of Al content in β-$Ni(OH)_2$, the current intensity of anodic peaks and cathodic peaks increases correspondingly. In the meantime, it is found that the potential difference for the two-phase mixtures is smaller than that for pure β-$Ni(OH)_2$ species. Hence, for the $Al_xNi_{1-x}LDH$ electrode, the electrochemical reversibility and activity for the electrochemical redox reactions should be better. This may be ascribed to the inserted OH^- ions between the brucite-like sheets and interlayer species, suggesting that the good access of OH^- ions involved in the transition between $Ni(OH)_2$ and NiOOH species.

Fig. 4 compares the discharge curves of β-$Ni(OH)_2$, $Al_{0.013}Ni_{0.987}LDH$, $Al_{0.019}Ni_{0.981}LDH$, and $Al_{0.034}Ni_{0.966}LDH$ at a galvanostatic current density of 1 A g^{-1}. It should be pointed out that the oxygen evolution reaction occurred during the charge process,

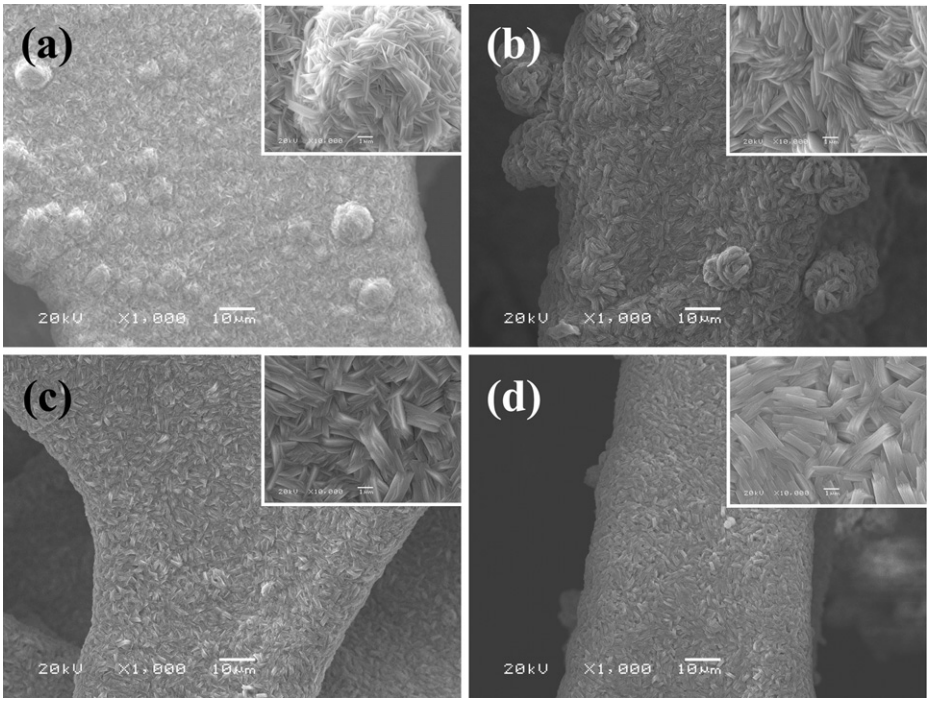

Fig. 2. The SEM images of the $Al_xNi_{1-x}LDH$ with x values of (a) 0, (b) 0.013, (c) 0.019, (d) 0.034.

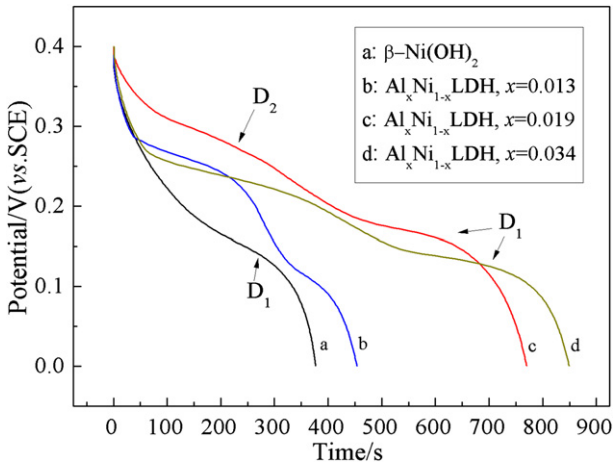

Fig. 4. The discharge curves of the Al_xNi_{1-x}LDH electrode at a galvanostatic current density of 1 A g^{-1}.

the actual charge/discharge potential range of 0–0.4 V. A single discharge plateau (D_1) is observed for pure β-Ni(OH)$_2$ electrode. The discharge plateau (D_1) of pure β-Ni(OH)$_2$ is about 0.15 V (Vs SCE) and close to that of $Al_{0.013}Ni_{0.987}$LDH. When the mol content of Al in β-Ni(OH)$_2$ was 1.9 mol% ($Al_{0.019}Ni_{0.981}$LDH) and 3.4 mol% ($Al_{0.034}Ni_{0.966}$LDH), the discharge plateau (D_1) are more flat and higher than that of pure β-Ni(OH)$_2$. This result can demonstrate that the discharge capacitance involved the transition between β-Ni(OH)$_2$/β-NiOOH for the Al_xNi_{1-x}LDH electrode are much higher than that of pure β-Ni(OH)$_2$ electrode. After the addition of Al, the additional discharge plateau (D_2) are observed, corresponding the reduction reaction of γ-NiOOH to α-Ni(OH)$_2$. The discharge plateau of α-phase Ni(OH)$_2$ are much higher than that of the β-phase Ni(OH)$_2$. This could attributed to larger quantity of water molecules within the interlayer space of α-phase Ni(OH)$_2$, which might be favorable to the proton diffusion during the charge/discharge processes [29,31]. These results are in good agreement with the two cathodic peaks changes as shown in Fig. 3.

Fig. 5 shows the influence of discharge current density on the specific capacitance of the β-Ni(OH)$_2$, $Al_{0.013}Ni_{0.987}$LDH, $Al_{0.019}Ni_{0.981}$LDH, and $Al_{0.034}Ni_{0.966}$LDH electrode. The specific capacitance was calculated according to the following equation:

$$C_m = \frac{I_d \times \Delta t}{\Delta V} \quad (1)$$

Where C_m (F g^{-1}) is the specific capacitance, I_d (A g^{-1}) is the discharge current density, Δt (s) is the discharge time and ΔV (V) is the discharge potential range. The specific capacitances at different discharge current densities were obtained from Fig. 5, and are listed in Table 2. As shown in Table 2, the maximum specific capacitance of pure β-Ni(OH)$_2$ electrode is 941.7 F g^{-1} at a discharge current density of 1 A g^{-1}. After the addition of Al, the specific capacitance of the Al_xNi_{1-x}LDH electrode are much higher than that of pure β-Ni(OH)$_2$ electrode. The $Al_{0.034}Ni_{0.966}$LDH electrode exhibits highest specific capacitance of 2122.6 F g^{-1} at a current density of 1 A g^{-1}. As we can see that when the discharge current density increases from 1 A g^{-1}

Table 2
The specific capacitance of the β-Ni(OH)$_2$, $Al_{0.013}Ni_{0.987}$LDH, $Al_{0.019}Ni_{0.981}$LDH and $Al_{0.034}Ni_{0.966}$LDH at different discharge current densities (corresponding to Fig. 5).

Specific capacitance (F g^{-1}) Al_xNi_{1-x}LDH	I_d (A g^{-1}) 1	I_d (A g^{-1}) 2	I_d (A g^{-1}) 4	I_d (A g^{-1}) 6
β-Ni(OH)$_2$	941.7	782.6	572.1	394.3
$x = 0.013$	1134.5	1007.8	864.7	957.3
$x = 0.019$	1924.5	1636.5	1387.9	1186.5
$x = 0.034$	2122.6	1742.6	1340.1	1389.4

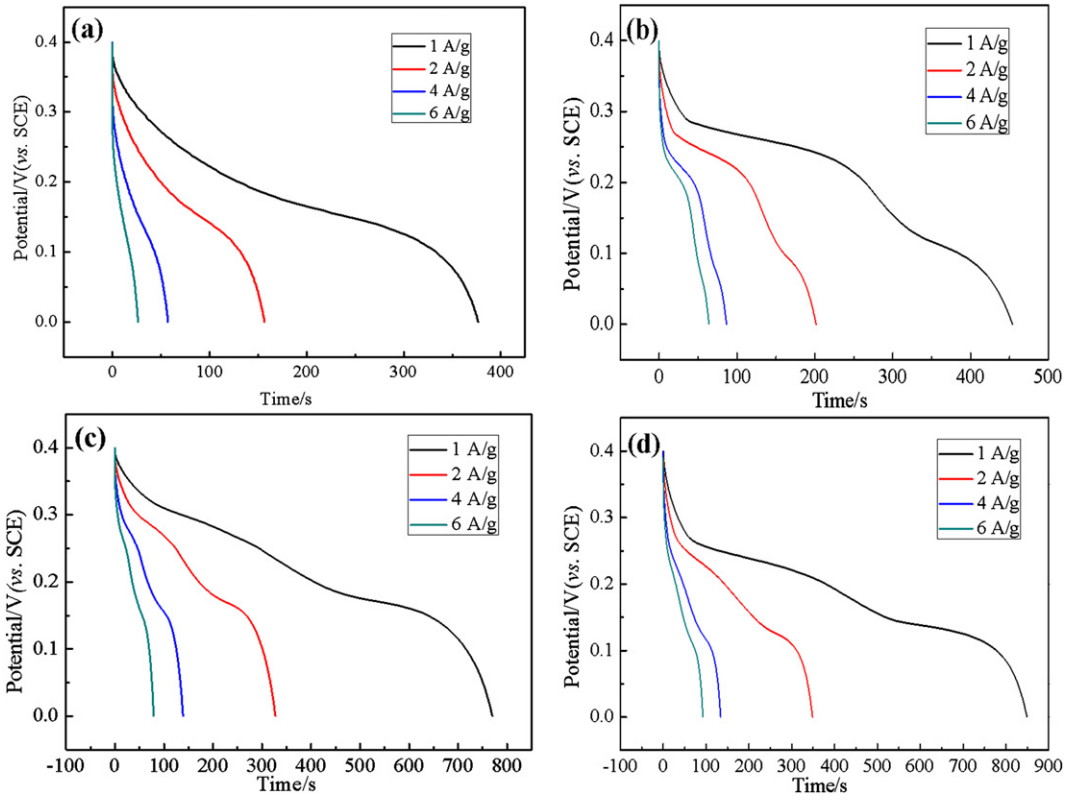

Fig. 5. The discharge curves of the Al_xNi_{1-x}LDH electrode at different current densities. (a) $x = 0$, (b) 0.013, (c) 0.019, (d) 0.034.

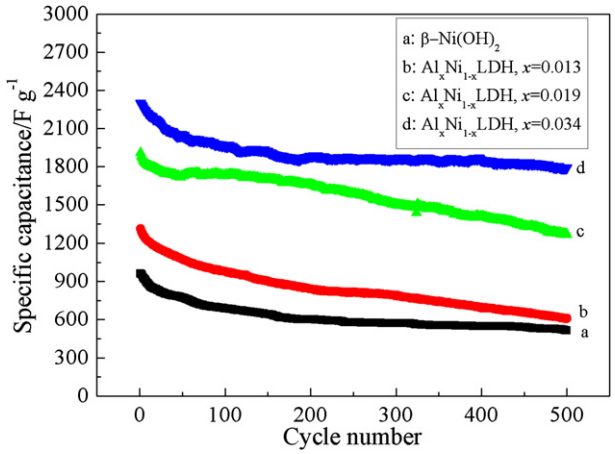

Fig. 6. Cycle performance of the Al_xNi_{1-x}LDH electrode at a galvanostatic current density of 1 A g^{-1}.

to 6 A g^{-1}, the capacitance for pure β-Ni(OH)$_2$ electrode decreases from 941.7 F g^{-1} to 394.3 F g^{-1}, while that for the $Al_{0.034}Ni_{0.966}$LDH electrode maintains a high level of 1389.4 F g^{-1}. The capacitance retention was found to be 41.8% and 65.4% for pure β-Ni(OH)$_2$ and $Al_{0.034}Ni_{0.966}$LDH, respectively. The electron storage mechanism of Ni(OH)$_2$ is dependent on redox reaction via OH^- ions and protons at the interface between Ni(OH)$_2$ and the KOH electrolyte. The enhancement of pseudocapacitive properties at a higher charging/discharging rate might due to its unique two-phase mixtures structure which provides good access of OH^- ions and water to the Ni(OH)$_2$ edge planes and thus to the interlayer.

The cycle performance of β-Ni(OH)$_2$, $Al_{0.013}Ni_{0.987}$LDH, $Al_{0.019}Ni_{0.981}$LDH, and $Al_{0.034}Ni_{0.966}$LDH electrode at 1 A g^{-1} are shown in Fig. 6. In the first 50 cycles, the discharge specific capacitance for all electrodes decreased obviously. After 200 cycles, the specific capacitance for all electrodes gradually stabilized at a slant plateau. For pure β-Ni(OH)$_2$ electrode, the capacitance retention was found to be only 53.5% after the 500 cycles, While that for the $Al_{0.034}Ni_{0.966}$LDH electrode maintains 78%. The results demonstrated the as-prepared $Al_{0.034}Ni_{0.966}$LDH electrode displayed a higher the pseudocapacitance than pure β-Ni(OH)$_2$ electrode.

In general, the electrochemical impedance spectroscopy measurements were used to investigate the reaction kinetics. EIS of the

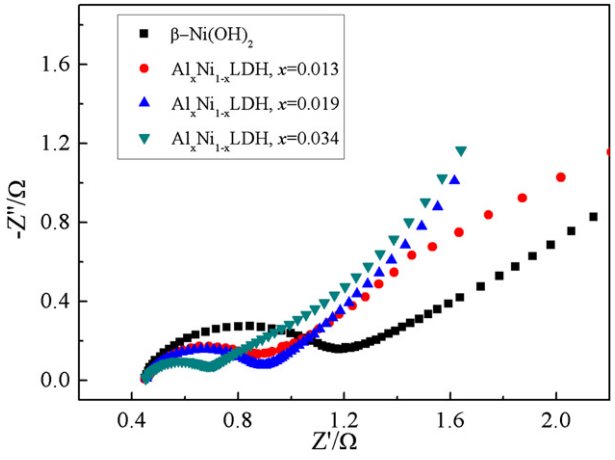

Fig. 7. The electrochemical impedance spectrum of the Al_xNi_{1-x}LDH electrode measured at the open circuit potential.

β-Ni(OH)$_2$, $Al_{0.013}Ni_{0.987}$LDH, $Al_{0.019}Ni_{0.981}$LDH, and $Al_{0.034}Ni_{0.966}$LDH electrode were measured at open circuit potential and the Nyquist plots were shown in Fig. 7. The impedances of all electrodes consist of a depressed semicircle in high frequency regions. Generally, the semicircle reflects the electrochemical reaction impedance of the electrode. Obviously, the Al-doped β-Ni(OH)$_2$ electrode exhibits a much smaller semicircle. The EIS results show the $Al_{0.034}Ni_{0.966}$LDH electrode has a lower charge transfer resistance and ion diffusion resistance with fast reaction kinetics.

4. Conclusions

Al-doped β-Ni(OH)$_2$ electrodes were prepared by a simple hydrothermal process. Al-doped β-Ni(OH)$_2$ electrodes exhibit much better electrochemical capacitance than the pure β-Ni(OH)$_2$ electrode. The $Al_{0.034}Ni_{0.966}$LDH electrode exhibits highest specific capacitance of 2122.6 F g^{-1} at a current density of 1 A g^{-1}. The enhancement of pseudocapacitive properties is due to its unique two-phase mixtures structure. The as-prepared $Al_{0.034}Ni_{0.966}$LDH electrode has a promising future as higher charging/discharging rate materials for pseudo-supercapacitors.

Acknowledgments

We gratefully acknowledge the financial support of this research by Fundamental Research Funds for the Central Universities (HEUCFT1205), the Postdoctoral Science-Research Developmental Foundation of Heilongjiang Province (LBQ-Q11149), Harbin Science and Technology Innovation Fund for Excellent Academic Leaders (2012RFXXG103) and Specialized Research Fund for the Doctoral Program of Higher Education (20102304110001).

References

[1] A. Burke, Electrochimica Acta 53 (2007) 1083–1091.
[2] A. Burke, Journal of Power Sources 91 (2000) 37–50.
[3] P. Simon, Y. Gogotsi, Nature Materials 7 (2008) 845–854.
[4] Y. Zhai, Y. Dou, D. Zhao, P.F. Fulvio, R.T. Mayes, S. Dai, Advanced Materials 23 (2011) 4828–4850.
[5] J. Balach, M.M. Bruno, N.G. Cotella, D.F. Acevedo, C.A. Barbero, Journal of Power Sources 199 (2012) 386–394.
[6] C.-C. Hu, K.-H. Chang, M.-C. Lin, Y.-T. Wu, Nano Letters 6 (2006) 2690–2695.
[7] S.K. Meher, G.R. Rao, Journal of Power Sources 215 (2012) 317–328.
[8] Y.-F. Lee, K.-H. Chang, C.-C. Hu, Y.-H. Chu, Journal of Power Sources 206 (2012) 469–475.
[9] G. Wang, J. Huang, S. Chen, Y. Gao, D. Cao, Journal of Power Sources 196 (2011) 5756–5760.
[10] J. Huang, H. Wu, D. Cao, G. Wang, Electrochimica Acta 75 (2012) 208–212.
[11] K. Xie, J. Li, Y. Lai, W. Lu, Z.a. Zhang, Y. Liu, L. Zhou, H. Huang, Electrochemistry Communications 13 (2011) 657–660.
[12] X. Zhao, C. Johnston, P.S. Grant, Journal of Materials Chemistry 19 (2009) 8755–8760.
[13] J. Huang, J. Zhu, K. Cheng, Y. Xu, D. Cao, G. Wang, Electrochimica Acta 75 (2012) 273–278.
[14] Y. Gao, S. Chen, D. Cao, G. Wang, J. Yin, Journal of Power Sources 195 (2010) 1757–1760.
[15] F. Zhang, C. Yuan, X. Lu, L. Zhang, Q. Che, X. Zhang, Journal of Power Sources 203 (2012) 250–256.
[16] T. Xue, X. Wang, J.-M. Lee, Journal of Power Sources 201 (2012) 382–386.
[17] F. Cao, G.X. Pan, P.S. Tang, H.F. Chen, Journal of Power Sources 216 (2012) 395–399.
[18] A.I. Inamdar, Y. Kim, S.M. Pawar, J.H. Kim, H. Im, H. Kim, Journal of Power Sources 196 (2011) 2393–2397.
[19] J. Yan, Z. Fan, W. Sun, G. Ning, T. Wei, Q. Zhang, R. Zhang, L. Zhi, F. Wei, Advanced Functional Materials 22 (2012) 2632–2641.
[20] G.-W. Yang, C.-L. Xu, H.-L. Li, Chemical Communications (2008) 6537–6539.
[21] Y. Yan, Q. Cheng, G. Wang, C. Li, Journal of Power Sources 196 (2011) 7835–7840.
[22] G. Wee, O. Larsson, M. Srinivasan, M. Berggren, X. Crispin, S. Mhaisalkar, Advanced Functional Materials 20 (2010) 4344–4350.
[23] Z. Liu, R. Ma, M. Osada, N. Iyi, Y. Ebina, K. Takada, T. Sasaki, Journal of the American Chemical Society 128 (2006) 4872–4880.
[24] E. Scavetta, B. Ballarin, C. Corticelli, I. Gualandi, D. Tonelli, V. Prevot, C. Forano, C. Mousty, Journal of Power Sources 201 (2012) 360–367.

[25] Z. Gao, J. Wang, Z. Li, W. Yang, B. Wang, M. Hou, Y. He, Q. Liu, T. Mann, P. Yang, M. Zhang, L. Liu, Chemistry of Materials 23 (2011) 3509–3516.
[26] V. Gupta, S. Gupta, N. Miura, Journal of Power Sources 177 (2008) 685–689.
[27] V. Gupta, S. Gupta, N. Miura, Journal of Power Sources 189 (2009) 1292–1295.
[28] Z. Lu, W. Zhu, X. Lei, G.R. Williams, D. O'Hare, Z. Chang, X. Sun, X. Duan, Nanoscale 4 (2012) 3640–3643.
[29] L.J. Yang, X.P. Gao, Q.D. Wu, H.Y. Zhu, G.L. Pan, The Journal of Physical Chemistry C 111 (2007) 4614–4619.
[30] Y. Wang, D. Cao, G. Wang, S. Wang, J. Wen, J. Yin, Electrochimica Acta 56 (2011) 8285–8290.
[31] W.-K. Hu, D. Noréus, Chemistry of Materials 15 (2003) 974–978.
[32] H. Chen, J.M. Wang, T. Pan, Y.L. Zhao, J.Q. Zhang, C.N. Cao, Journal of Power Sources 143 (2005) 243–255.
[33] G.A. Caravaggio, C. Detellier, Z. Wronski, Journal of Materials Chemistry 11 (2001) 912–921.
[34] X.Y. Wang, H. Luo, P.V. Parkhutik, A.C. Millan, E. Matveeva, Journal of Power Sources 115 (2003) 153–160.